Article:
Wade, A, Copley, R, Clarke, B et al. (4 more authors) (2020) Real-time fretting loop regime transition identification using acoustic emissions. Tribology International, 145. 106149. ISSN 0301-679X

https://doi.org/10.1016/j.triboint.2019.106149

Title

Real-Time Fretting Loop Regime Transition Identification Using Acoustic Emissions

Authors

A. Wade[a], R. Copley[b], B. Clarke[b], A. Alsheikh Omar[a], A. R. Beadling[a], T. Liskiewicz[c] and M. Bryant[a]

[a] *University of Leeds, School of Mechanical Engineering, Institute of Functional Surfaces, Leeds, UK;*

[b] *University of Sheffield, School of Mechanical Engineering, Leonardo Tribology Centre, Sheffield, UK;*

[C] *Manchester Metropolitan University, Faculty of Science and Engineering, Manchester, UK.*

Abstract

Acoustic emission (AE) has been successfully used to investigate the damage mechanisms of fretting contacts within different regimes. This study investigated the transition between fretting regimes using the relationship between AE and the mechanical response of a dry, steel-on-steel, ball-on-flat contact under different tangential displacements achieving the partial slip regime, mixed fretting regime and gross slip regime. Increased AE response occurred during gross-slip events and there was strong positive correlation between AE and fretting energy ratio. The relationship was strongest when gross sliding was experienced allowing identification of transition from the partial slip to the gross slip regime. This makes AE a good candidate to detect regime transition in-situ due to ease of integration and its non-destructive nature.

Keywords/Phrases

Fretting regime, transition, correlation, acoustic emissions

1. Introduction

Fretting is “a special wear process that occurs at the contact area between two materials under load and subjected to minute relative motion by vibration or some other force” according to the American Society of Metals [1]. The nature of fretting means that detection is difficult, resulting in either catastrophic failure or expensive maintenance programmes [2,3]. Catastrophic failure like that seen in the lap joints and rivets of a fuselage leading to the Aloha Airlines accident [4]. Fretting occurs in many systems that are subject to cyclic loads such as: suspension cables, dovetail joints in turbine engines, electrical contacts and heat exchangers [5]. Fretting contacts are extremely complex, transient in nature and intimately linked with corrosion leading to a complex degradation mechanism [6,7]. Orthopaedic implants are one such example where fretting-corrosion is a significant degradation mechanism leading to early failure [8,9]. Depending on the working conditions, different fretting regimes can be achieved and are associated with different degradation mechanisms [10]. The partial slip regime (PSR) is more commonly associated with fretting fatigue crack formation and the gross slip regime (GSR) with fretting wear and material removal. Identification of the regime is important in understanding the dominant degradation mechanism [11].

Considering a Hertzian contact, different fretting regimes demonstrate characteristic fretting loops and material responses [10,11]. Fretting loops characteristic of the PSR demonstrate a narrow hysteresis loop associated with plastic shear and fatigue crack formation. Mindlin[12] was the first to introduce the presence of a central stick region with limited degradation due to sufficient normal stress to prevent slip, surrounded by an outer slip region where normal stress is insufficient in preventing slip. The GSR fretting loops display a larger, elongated hysteresis loop associated with surface and bulk plastic deformation coupled with fracture at all the connecting asperities. The mixed fretting regime (MFR) is

where transition between the GSR and PSR exists under constant working conditions close to critical values of tangential displacement (δ) and normal load (W), resulting in highly transient and unpredictable processes at the interface [13]. Differentiation between regimes is commonly achieved using criteria directly derived from the characteristic parameters of fretting loops such as fretting energy dissipation (ratio, A), slip ratio (D) and slip index (δ_i) [14–21]. Therefore, accurate measurement and analysis of the material response are essential for correlation with other datasets.

Acoustic emission (AE) has been used as a method of non-destructive testing (NDT) as early as the 1960s and has allowed online monitoring of engineering components [22,23]. This has been used to monitor tribological components such as high speed cutting tools and rolling elements bearings using piezoelectric transducers [24,25]. AE is defined as transient elastic wave generated by the rapid release of energy in a localised source within a material [26]. This can be caused by any activities resulting in the transfer of energy including crack formation and propagation, dislocations, leakages, corrosion, material impingement and fracture of contacting asperities [26–30]. AE can either be burst or continuous in nature depending on the acoustic stimulation, meaning characterisation can differ [26].

AE techniques have been used to monitor tribological activities under different sliding conditions in both lubricated and non-lubricated systems. Fatigue crack initiation and propagation has been investigated using the number of burst signals (hits) [31]. Three distinct stages were identified by the rate of recorded hits as initiation, plastic response at the crack tip followed by shearing between micro-voids. Wear processes have also been investigated using AE [32,33]. The root mean square voltage of acoustic hits has been found to increase with increased specific wear rate [32]. Differences in AE response have also been found between adhesive and abrasive wear mechanisms [33]. Consistent with other studies both mechanisms presented an increase hit amplitude with increased transfer particles and wear elements due to the sudden release of strain energy. However, the frequency spectra of these hit signals differed between wear mechanisms associated with the variance in wear particles produced. Sliding contacts that experienced stick-slip phenomena produced an increased hit amplitude during the onset of slip (transition from static to kinetic friction), associated with the sudden release of contacting asperities [30,34]. This explanation also follows for lubricated systems. Contacts under a mixed lubricated regime (i.e. asperity contacts are present) increased AE intensity was found with increasing load and speed associated with the increase rapid release of strain energy of contacting asperities [35].

Fretting contacts have also been investigated using AE techniques. Fretting fatigue crack formation was investigated using AE with an applied tensile force to the flat specimen and a fretting motion using a Hertzian contact in the PSR [27,36,37]**.** There was found to be an increased accumulative energy and number of hits associated with the rapid release of strain upon crack initiation and propagation. However, it was clear that correlation between mechanical data, wear morphology and acoustic data was difficult, often only comparing general trends as opposed to specific events in data sets. Fretting wear was investigated by Ito et al. [38] using a metal-on-metal contact finding that peaks in AE amplitude did not occur in the PSR but occurred in the GSR when pure slip was achieved, associated with the sudden fracture of contacting asperities. This was also seen in another fretting wear study that used a ductile metal-on-metal contact, that found increased hits during the sliding portion of the GSR fretting loop at the start of the test [39]. However, as the experiment progressed ploughing action of the contact resulted in the increased amplitude of the hits at the loop extremities. Effects of the ploughing action was also seen in fretting experiments using ceramic-on-metal contacts, identifying collision with the ends of the wear tracks as a possible source of AE [40]. Although there have been studies carried out to help the understanding of fretting contacts using AE, there appears to be a lack of accurate

correlation of mechanical data with acoustic signals for the purposes of regime transition identification.

This study aimed to develop a fretting wear model with integrated AE sensing capability with the view correlate AE signals with the mechanical response of a fretting contact to identify fretting regimes. This was achieved by correlating the mechanical response of the fretting contact and the fretting energy ratio (A) with AE signals in real-time. This has a number of applications including the development of asset monitoring devices, enabling smart monitoring due to the ease of incorporation of AE sensors into systems.

2. Materials and Methods

2.1 Experimental set up

A bespoke in-house built fretting tribometer, coupled with an acoustic emission (AE) sensing system, was used in this study. A 3D schematic of the experimental set up can be seen in Figure 1. The fretting rig applied oscillatory tangential displacements through an electrodynamic shaker (GWV55/PA300E, Signal Force). Normal load (W) was applied by a cantilever system through the contact interface.

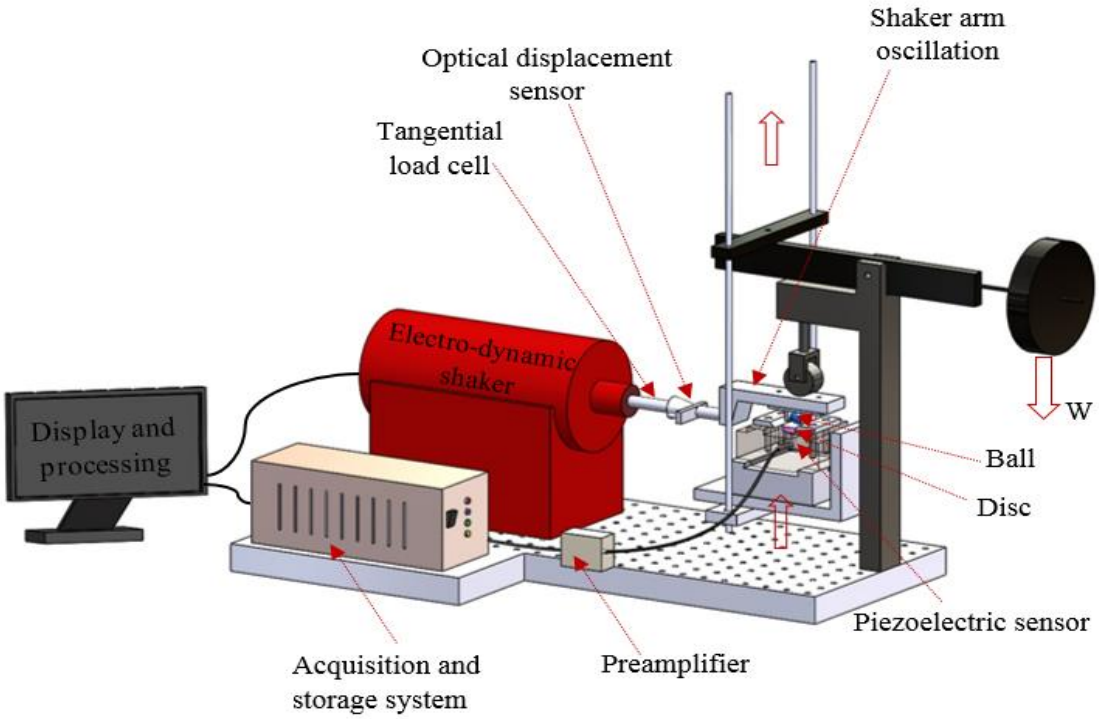

Figure 1: 3D Schematic of experimental set up.

Fretting output data included tangential load (Q) and tangential displacement (δ) which were measured using an axially mounted load cell and optical displacement sensor respectively. The device was controlled, and data recorded by means of a custom LabVIEW (National Instruments, USA) programme. The contact geometry was a bearing steel ball, $\emptyset 12.7\ mm$ (E_{ball} = 180 GPa, v_{ball} = 0.3) on a flat X65 carbon steel disk (E_{flat} = 200 GPa, v_{flat} = 0.3). A disc sample holder was designed to allow the contacting interface to be monitored with a piezoelectric sensor (VS900-M, Vallen Systeme GmbH), as shown in Figure 2.

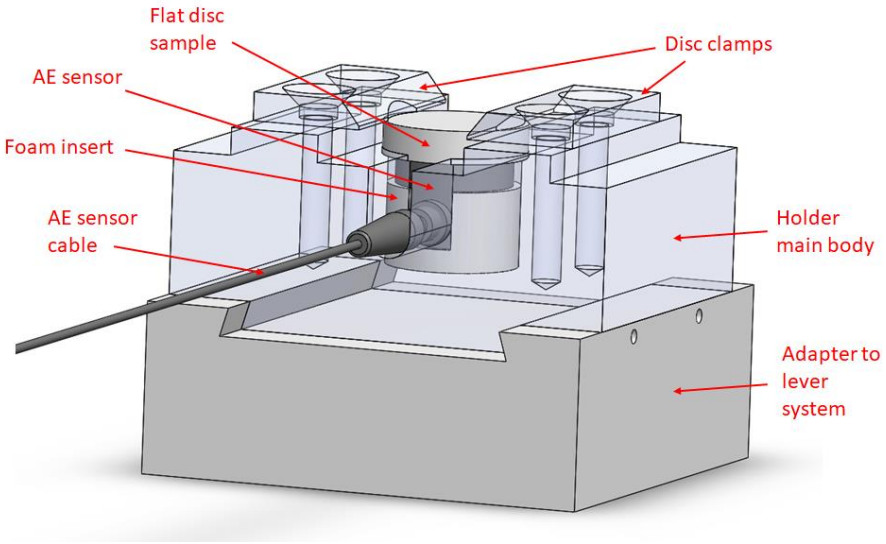

Figure 2: Detailed view of how the AE sensor was integrated into the fretting rig

The sensor-disc interface was mediated by a thin layer of vacuum grease. The piezoelectric sensor converted AE signals into electric signals. The electrical signals were then passed through a preamplifier (AEP4H, Vallen Systeme GmbH) which amplified and filtered the electrical signals before processing in an acquisition and storage system (AMSY-6, Vallen Systeme GmbH) and displayed by software. Prior to experimental evaluation, a thresholding activity was conducted to ensure AE events detected were those arising from the interface appose to the fretting equipment. Tribometer and AE sensing experimental parameters can be seen in Table 1.

Table 1: The values of fretting and acoustic emission (AE) set up parameters.

Fretting parameters	**Values**	**AE parameters**	**Values**
Normal load (N)	50	TR recording rate (MHz)	2.5
Number of cycles	1500	Threshold (dB)	20
Hertzian contact pressure (MPa)	917	Acquisition frequency (MHz)	10
Tangential displacements (μm)	25, 50, 75, 100	Preamplifier frequency (kHz)	90-850
Frequency (Hz)	3		

The fretting displacement reached steady state for all experiments after a period of running-in which was determined as the point at which the fretting rig achieved the selected displacement amplitudes and can be seen in the results section. In this study, different tangential displacement amplitudes (δ^*) were run with three repeats. Fretting data (Q and δ) and AE data (hit amplitudes in dB) was recorded simultaneously and exported for post analysis using MATLAB (MathWorks, USA). Figure 3 shows a schematic of an AE hit and associated amplitude from the raw AE single.

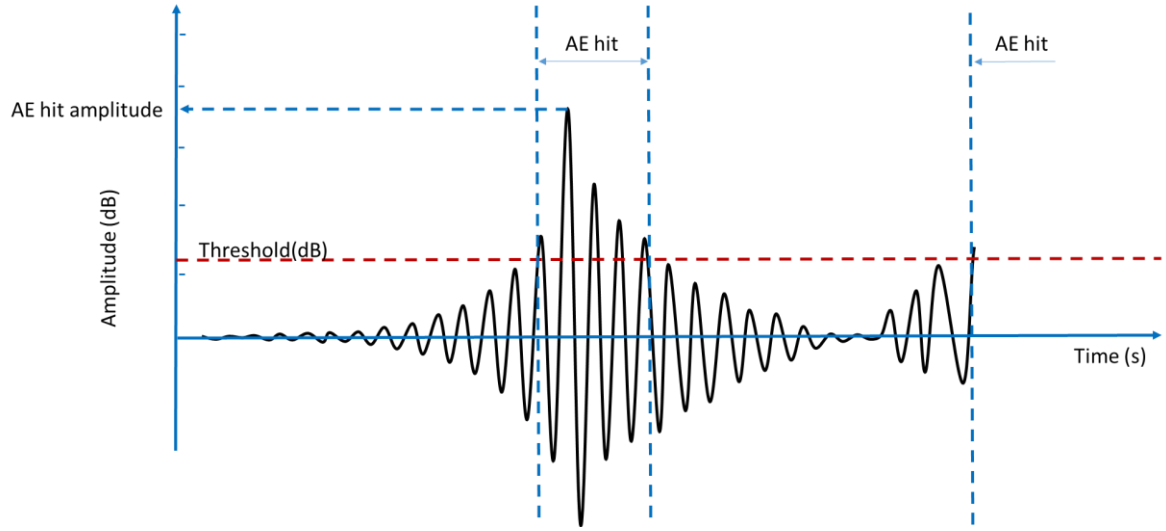

Figure 3: Schematic showing the raw AE signal with indicated AE hit and associated hit amplitude.

2.2 Correlation between fretting and AE data

Correlation of the fretting data with AE data was achieved by the ratio between dissipated energy (E_d) and total energy (E_t) i.e. the fretting energy ratio (A, see Equation 1).

$$A = \frac{E_d}{E_t} \qquad \textit{Equation 1}$$

E_d was calculated as the area bound by the fretting loop using the "polyarea" MATLAB function. E_t was approximated as the area of the smallest rectangle able to contain each fretting loop. Figure 4 shows a schematic of both E_d and E_t.

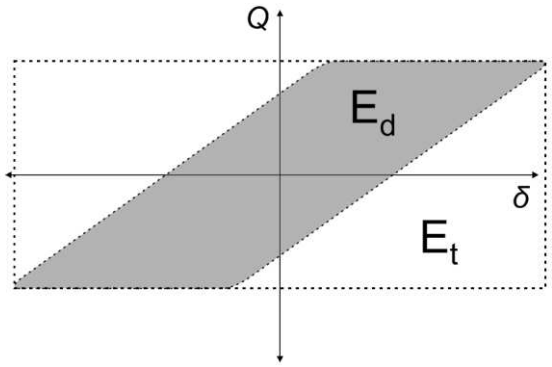

Figure 4 Schematic of dissipated energy (E_d) and total energy (E_t).

Transition between the PSR and GSR was identified by the energy ratio threshold of 0.2. This threshold was identified by Fouvry et al. [17], where a ratio of 0.2 identifies the theoretical point at which static friction is overcome based on Mindlin's formalism. Above the threshold indicates an increased proportion of dissipated energy due to a sufficient tangential force to overcome static friction of the contact. While a ratio below the threshold indicates a higher proportion of recovered elastic energy due to insufficient tangential force to overcome static friction at the contact.

This data was synchronised with the maximum AE hit amplitude for each second using time-date stamps. The correlation between energy ratio and AE hit amplitude was quantified by using a Pearson's correlation coefficient. Pearson's correlation analysis was performed using data from the

experiment, including prior to the fretting rig reaching steady state. This provided a single variable to quantify how well the mechanical response of the fretting contact linearly correlated with AE hit amplitude during the progression of the whole experiment, including during times of transition prior to reaching steady state. Deeper analysis of the AE data was performed and compared to fretting data on a sub-loop scale. This was achieved by plotting each hit and its corresponding amplitude against two coordinates 1) position within a the loop and 2) cycle number.

3. Results

3.1 Sub-loop AE Response

Increased AE hit amplitude occurred when gross-slip at the interface was achieved. This can be seen in Figure 5 where an increased AE hit amplitude corresponded to slip events identified as regions of constant Q independent of sliding velocity. The δ^* = ± 25 μm experiment did not experience gross-slip and a corresponding constant AE hit amplitude of around 25 dB was observed (Figure 5a). The δ^* = ± 50 μm, δ^* = ± 75 μm and δ^* = ± 100 μm experiments did experience gross-slip shown by the periods of approximately constant Q (Figure 5b, c and d respectively). During these periods of constant Q and increasing δ, increased hit amplitude was observed with increasing tangential displacement (δ). Under a constant normal force of 50 N slip was generally achieved at a tangential force of ± 10 N, resulting in a static coefficient of friction of approximately 0.2.

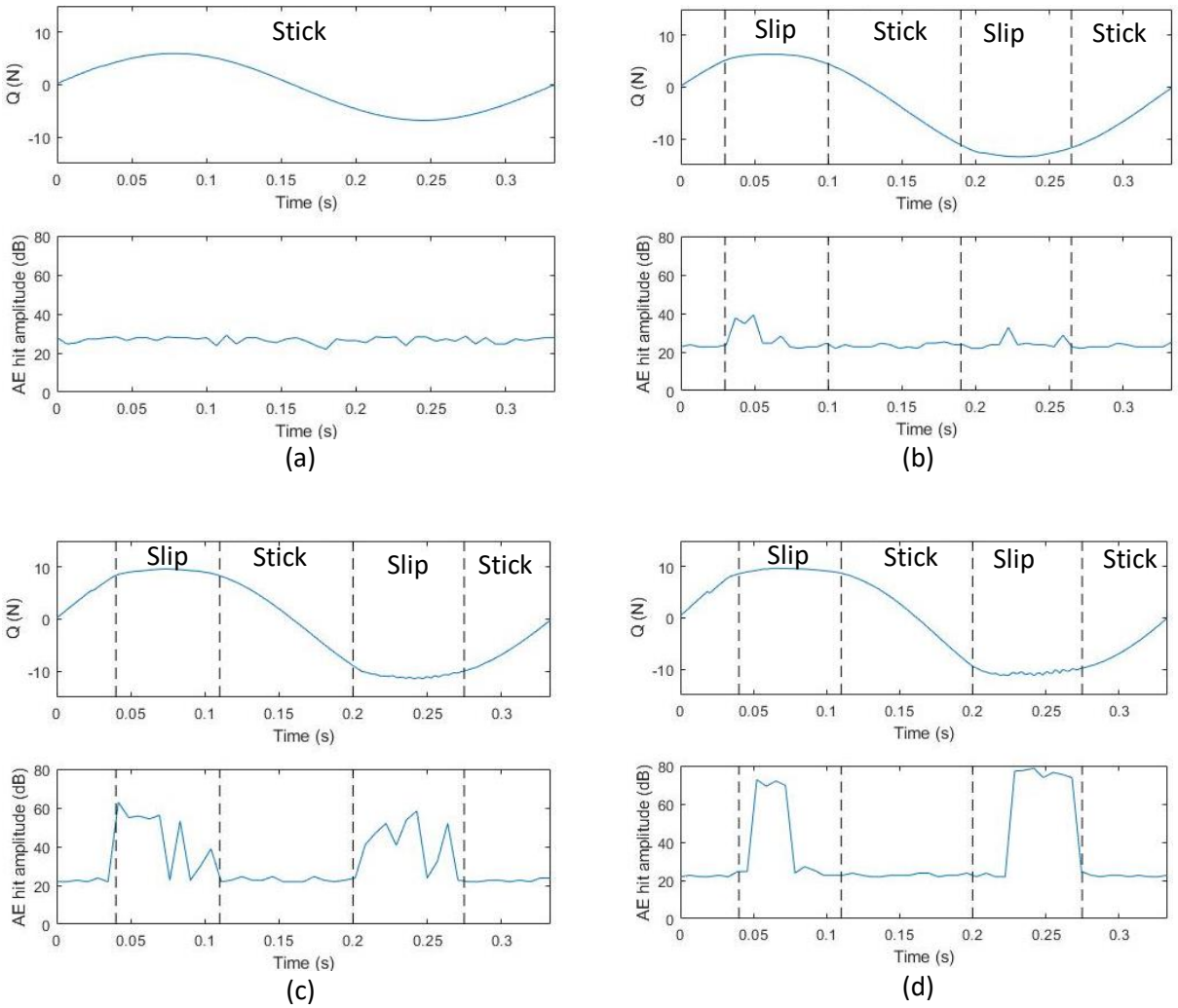

Figure 5: Tangential displacement (Q) synchronised with AE hit amplitude verses time within a cycle for the: (a) $\delta^* = \pm 25$ μm experiment (b) $\delta^* = \pm 50$ μm experiment, $\delta^* = \pm 75$ μm experiment and $\delta^* = \pm 100$ μm experiment.

3.2 Loop-by-loop AE Response

The selected tangential displacements for the given working conditions presented the PSR, GSR and a mixture of the two. Typical examples of each experiment are shown in Figures 5-8, each of which is split into three parts. These are (a) Q-δ plots throughout the experiment, (b) comparisons of energy ratio and AE and (c) spectral maps showing AE hit activity as a function of cycle position and cycle number.

Figure 6a demonstrates a PSR response throughout the whole experiment for $\delta^* = \pm 25\ \mu m$. Energy ratio remained well below the 0.2 threshold indicating the PSR. The AE hit amplitude remained consistently low between $23 - 26\ dB$ throughout the whole experiment shown in both Figure 6b and c.

(a)

(b)

(c)

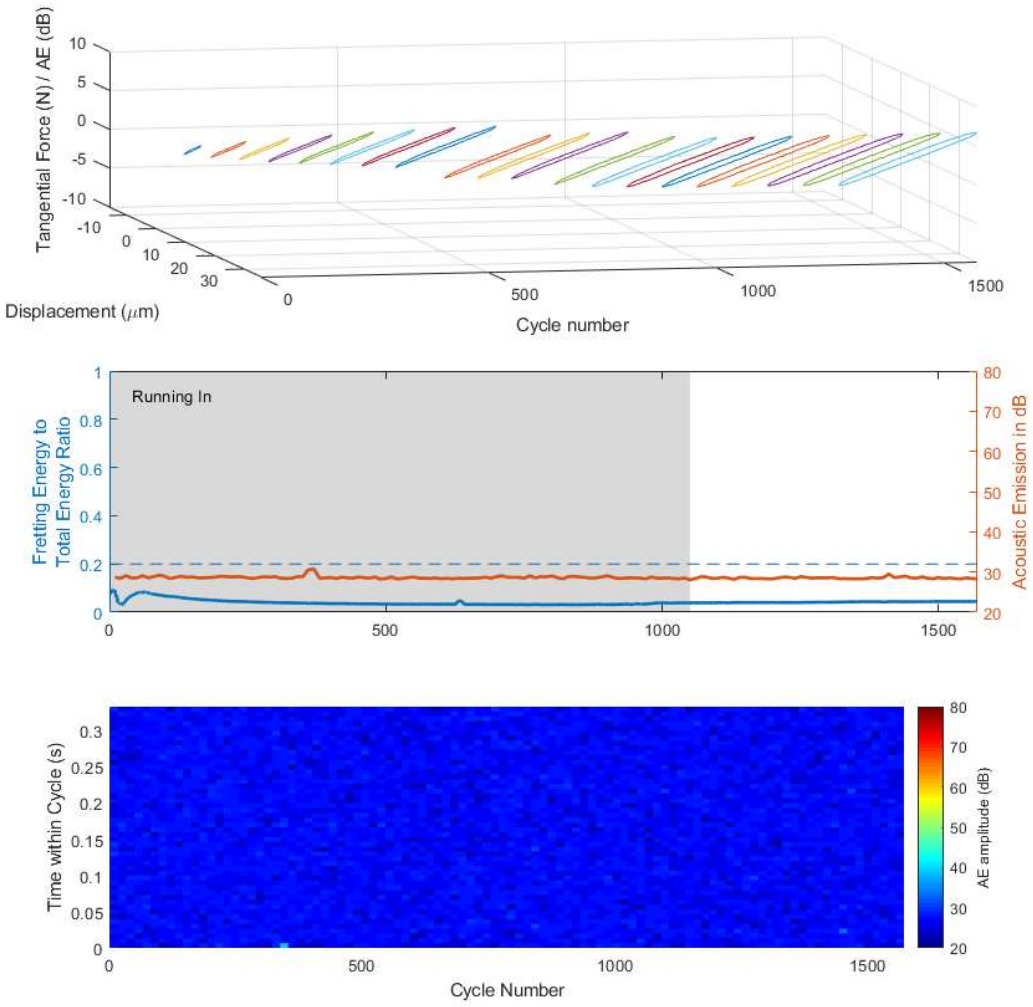

Figure 6: The $\delta^* = \pm 25$ μm experiment (a) fretting loops, (b) energy ratio (A) and AE hit amplitude and, (c) Sub-loop AE hit amplitude over the whole experiment.

In the δ^* = ± 50 μm experiment, the contact was within the MFR. This was demonstrated by narrow hysteresis loops, which transitioned after the running-in period, shown in Figure 7a. This was demonstrated by energy ratio crossing the 0.2 threshold indicating the static friction was overcome giving rise to the GSR. There was also a corresponding increase in AE hit amplitude that peaked to $56.32\ dB$, around $30\ dB$ above the relatively constant AE observed in the δ^* = ± 25 μm experiment. After transition small fluctuations in AE by approximately $2\ dB$ above that observed in the PSR. Figure 7c identifies two acoustic events per cycle that that were both greater at the onset of the GSR.

(a)

(b)

(c)

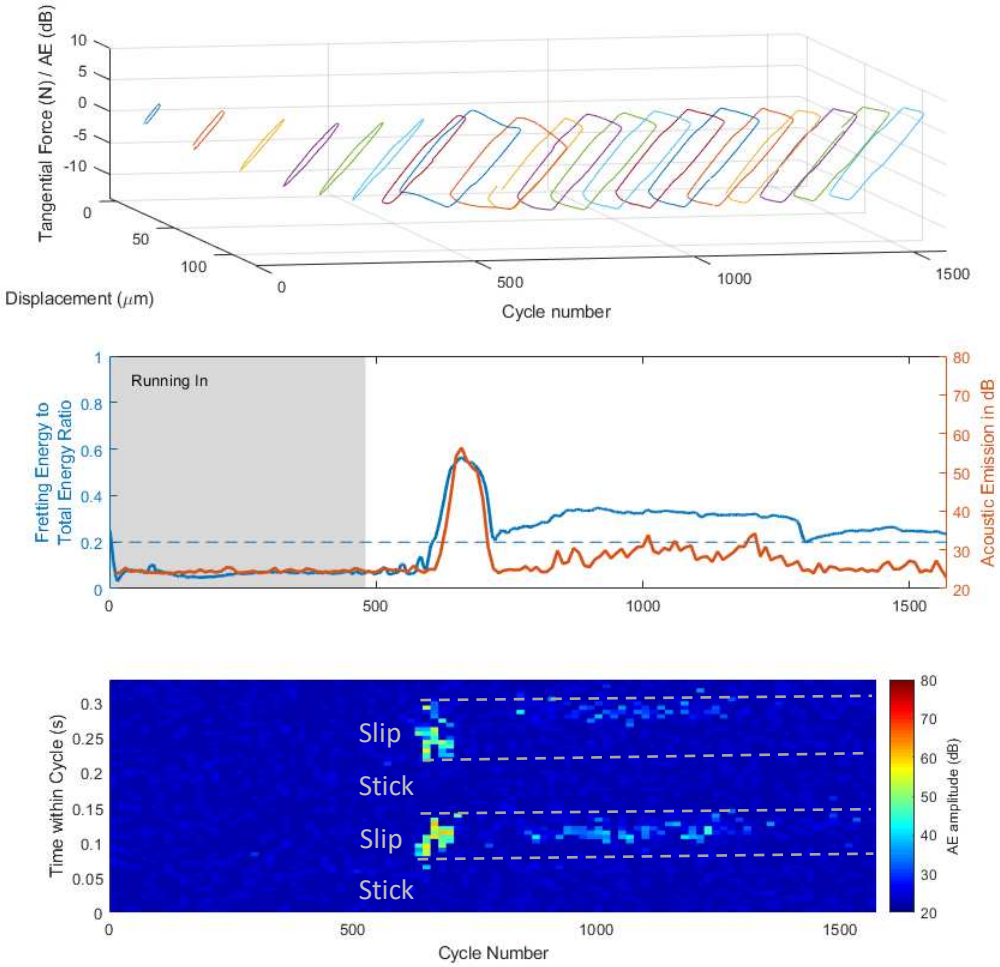

Figure 7: The $\delta^* = \pm 50\ \mu m$ experiment (a) fretting loops, (b) energy ratio (A) and AE hit amplitude and, (c) Sub-loop AE hit amplitude over the whole experiment with regions of stick and slip indicated.

The δ^* = ±75 µm experiment was in the GSR as transition occurred within the running-in period demonstrated by the Q-δ plots and energy ratio (Figure 8a and b respectively). This transition at around 240 cycles demonstrated a gradual increase in energy ratio accompanied by a simultaneous increase in AE hit amplitude to around $45\ dB$. After transition the energy ratio varied between 0.5-0.6 and a greater AE hit amplitude between $45 - 65\ dB$, greater than the δ^* = ± 50 µm. Two acoustic events occur per cycle, both events present a gradual increase to a similar amplitude as the experiment progressed as shown in Figure 8c.

(a)

(b)

(c)

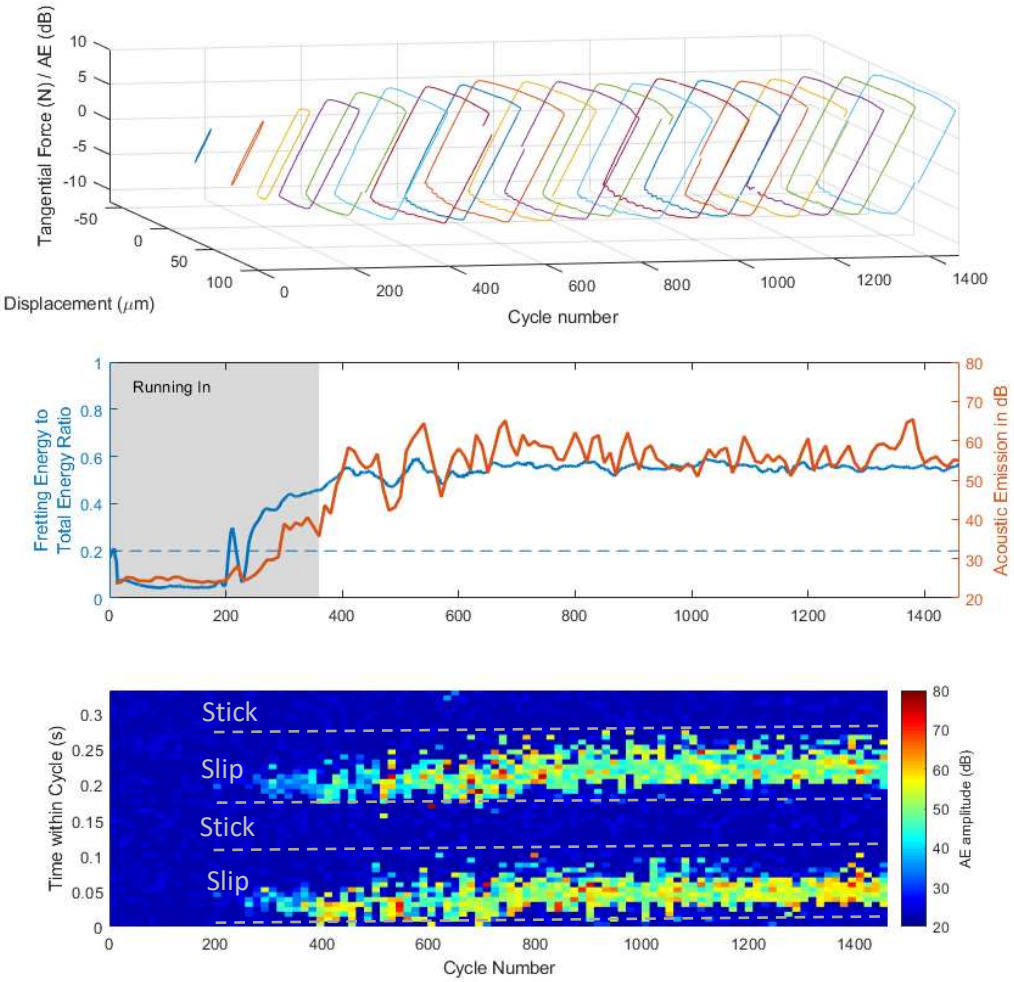

Figure 8: The $\delta^* = \pm 75\ \mu m$ experiment (a) fretting loops, (b) energy ratio (A) and AE hit amplitude and, (c) Sub-loop AE hit amplitude over the whole experiment with regions of stick and slip indicated.

The δ^* = ±100 μm experiment was in the GSR with the hysteresis loops displaying a larger proportion of pure slip than the δ^* = ±75 μm (Figure 9a). There was a corresponding greater energy ratio between $0.6 - 0.7$ and AE hit amplitude $65 - 80\ dB$ (Figure 9b). Additional to the relationship between energy ratio and AE amplitude seen upon transition, events within the GSR were also identified at cycle number 1000 and 1300 (Figure 9b and c). This was seen within the energy ratio but was more noticeable from the AE response. Unlike the δ^* = ±75 μm experiment increases in energy ratio beyond the threshold occurred during the first 200 cycles without a corresponding increase in AE hit amplitude. Figure 9c also demonstrated that these events occurred twice within a loop with subtle differences between the two.

(a)

(b)

(c)

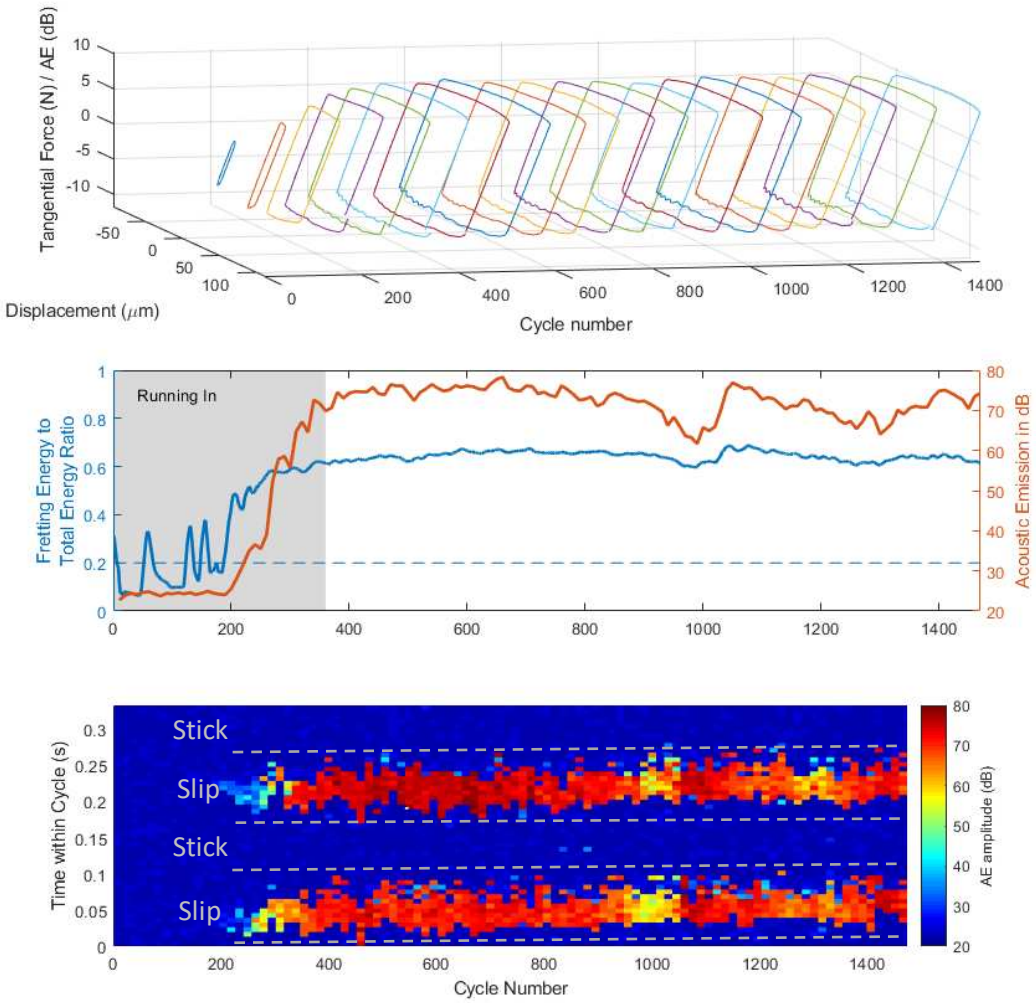

Figure 9: The $\delta^* = \pm 100\ \mu m$ experiment a) fretting loops, (b) energy ratio (A) and AE hit amplitude and, (c) Sub-loop AE hit amplitude over the whole experiment with regions of stick and slip indicated.

4. Discussion

This study found a correlation between AE response and transition of a fretting contact between the PSR and GSR. The results agree with those of Ito et al. [38] in that within the PSR acoustic energy was that of the background noise always present during fretting, but an increase in AE occurred in the GSR. In this study an increased hit amplitude occurred with gross-slip events (Figure 5). This resulted in a strong correlation between the fretting energy ratio and AE hit amplitude. This is shown in Figure 10 where a Pearson's correlation coefficient of 1 indicates a perfect positive linear correlation between fretting energy ratio and AE hit amplitude, while a coefficient of 0 indicates no correlation. The GSR experiments (δ^* = ± 75 μm and δ^* = ± 100 μm) demonstrated a very strong correlation due to the presence of gross-slip events and higher energy ratio. The MFR demonstrated a medium correlation strength as a smaller proportion of the experiment presented loops characteristics of the GSR. The δ^* = ± 25 μm experiments within the PSR and therefore an energy ratio below 0.2 presented little to no correlation due to the absence of gross-slip events resulting in a correlation coefficient of around 0.1.

However, one of the three $\delta^* = \pm 25\ \mu m$ experiments presented an a transient slip event which resulted in an anomalous correlation coefficient of 0.6 i.e. greater than three standard deviations from the mean of the other two. This relationship between AE hit amplitude and energy ratio was likely due to a the short duration of the experiments where fretting wear processes dominated. Over a longer test duration fretting fatigue and crack formation could occur, resulting in an increase AE response in the PSR affecting the correlations found during this study.

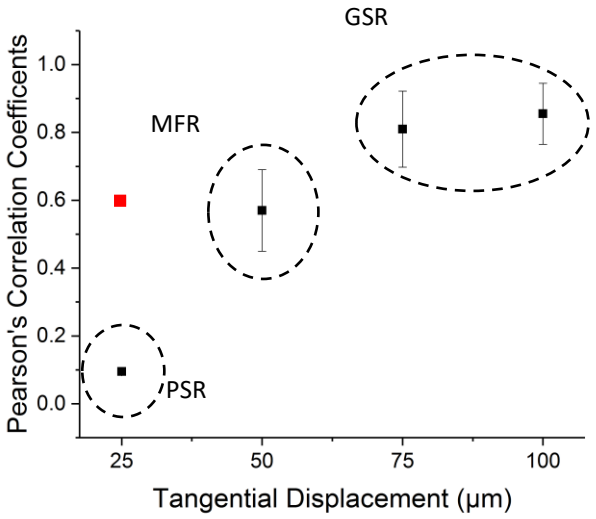

Figure 10 Pearson's correlation coefficient between fretting energy ratio and AE hit amplitude for experiments at each displacement. The error bars represent the 95% confidence intervals from the three repeats of each experiment.

The correlation was strongest during transition due to the proportional reduction in noise, particularly in the AE signal. The most likely source of AE was a result of the sudden release of contacting asperities upon the onset of gross slip at the interface. This is supported by the sub-loop AE analysis plots which shows two regions of acoustic activity per cycle, not present until pure slip was seen in the fretting loops. These two areas of increased AE activity per cycle are consistently separated by approximately 0.16 s which corresponds to the time for half a cycle running at 3 Hz. Additionally, the hit amplitude shows a general trend of increasing with tangential displacement amplitude when in the GSR. As the fretting frequency was kept constant during these experiments, the slipping speed increased with tangential displacement. Therefore the increased AE hit amplitude could be explained by a faster release of elastic strain energy from breaking asperity junctions, as suggested by Briscoe et al.[41]. This is also in agreement with an in-silico study that investigated a rough sliding contact [42]. This study found that the frequency of shocks due to contacting asperities per unit time decreased but the intensity increased. If the sliding speed was constant and the tangential displacement amplitude was increased one would expect an increase in the number of acoustic hits per cycle as more asperity junctions were formed and broken but not an increase in hit amplitude. An alternative explanation for AE is collisions at the ends of the wear track as seen in previous studies that employed ductile contacts that experienced ploughing [39]. The general trend of AE hit amplitude increasing with tangential displacement amplitude when in the GSR could then be explained by the higher energy impacts at higher sliding speeds. However, this was unlikely as suggested by the lack of hooked-like corners of the fretting loops and upon observation of the synchronised plots between Q and AE hit amplitude for a given cycle (Figure 5). This highlights a limitation of this study, only using hits to analyse the AE response which meant that the source of the AE could not be distinguished. Future work includes frequency spectra analysis of the AE response.

The δ^* = ±100 µm experiment also saw an observable relationship between AE and energy ratio after transition into the GSR around cycle numbers 1000 and 1300 (Figure 9b). Within gross-slip portions of the fretting loops (Figure 5d and Figure 9a) fluctuations were possibly due to the occurrence of stick-slip phenomena, a source of AE seen in other studies [30,34]. Conversely, within the MFR after an increase in AE hit amplitude was observed during the onset of gross-slip, a reduction thereafter was demonstrated. This effect was seen in previous studies due to the retention of wear debris within the contact, which led to the formation of a tribologically transformed structure layer during longer experiments [38,40,43]. This effect was not seen in the two experiments that demonstrated the GSR. One explanation is the expulsion of the wear debris from the contact at the larger displacements.

This δ^* = ±100 µm experiment also demonstrated points at which the fretting energy ratio exceeded the 0.2 threshold during the first 200 cycles without a corresponding increase in AE hit amplitude (Figure 9b). Deeper analysis of the fretting loops during this period reveal transient uncharacteristic mechanical responses shown in Figure 11a and b. This suggests an increased proportion of dissipated energy (E_d) that was not due to a pure slip event indicated by the gradient between Q and δ differing from characteristic fretting loops seen more clearly in Figure 11a. This was a limitation in using only one parameter to correlate the mechanical response to AE signals. Future work could include the use of a recently developed method by Wade et al. [44] that is able to quantify the different proportional responses of a fretting contact and identify any uncharacteristic responses.

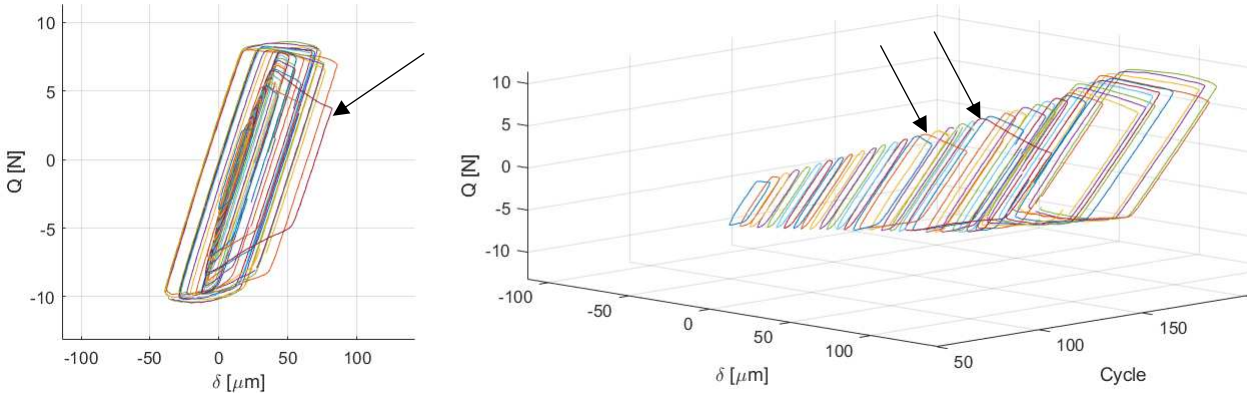

Figure 11 Fretting cycles during the first 200 cycles of the example $\delta^* = \pm 100$ µm experiment. (a) 2D plot of fretting loops (b) 3D plot of fretting loops against cycle number. Arrows indicate uncharacteristic fretting loops.

This study successfully correlated AE response with mechanical fretting data. Increased AE activity was observed during slip events and is therefore a good candidate to detect PSR to GSR transition in-situ. The challenge now lies in separating these AE signals from other signals from the contact and other sources within a system. Although activity and intensity are used to classify AE signals it has been shown that they are insufficient in resolving differences in features of the stress waves generated by different processes such as mechanical, chemical and thermal. This is where frequency spectra analysis can come in, where differences in frequency have been found to reflect friction and some wear [45]. The capacity of this technique to be used for online monitoring could be further enhanced by the use of different loop analysis methods. Like that developed previously providing further information of the mechanical response of the contact in real time with transition criteria independent of Amonton's third law [44].

5. Conclusion

The relationship between AE and the material response of a dry, steel-on-steel ball on flat fretting contact was examined under different tangential displacements achieving the PSR, MFR and GSR. There was strong positive correlation between AE and fretting energy ratio in the GSR and at transition from the PSR to the GSR. The PSR provided AE similar to that of the background noise always present during fretting and an increase in AE occurred in the GSR. This was due to an increased hit amplitude with the presence of gross-slip events causing a rapid release of elastic strain energy. The relationship between AE and energy ratio was strongest when gross sliding occurred and therefore transition from the PSR to the GSR which makes AE a good candidate to detect regime transition in-situ. One limitation of this study was the ability to distinguish between different AE events. Future work incudes of analysis of the frequency spectra and loop analysis methods that can provide more online information about the mechanical response of the contact.

6. Acknowledgements

Funding was provided by the EPSRC Centre for Doctoral Training for Integrated Tribology. Grant No. EPL01629X1.

7. Declaration of Interest Statement

There were no conflicts of interest.

8. References

1. ASM Handbook Committee. Fretting Fatigue. In: *Fatigue and Fracture*. Vol 19. 8th ed. ASM International; 1996:321-330. doi:10.31399/asm.hb.v19.a0002372
2. Makino T, Kato T, Hirakawa K. Review of the fatigue damage tolerance of high-speed railway axles in Japan. *Eng Fract Mech*. 2011;78(5):810-825. doi:10.1016/j.engfracmech.2009.12.013
3. Szolwinski MP, Farris TN. Mechanics of fretting fatigue crack formation. *Wear*. 1996;198(1-2):93-107. doi:10.1016/0043-1648(96)06937-2
4. National-Transport-Safety-Board. Aircraft Accident Report Aloha Airlines, Flight 243 Boaeing 737-200, Near Maui Hawaii, April 28 1988. 1989. doi:NTSB/AAR-89/03
5. Forsyth PJ. Fretting fatigue. In: Waterhouse RB (Robert B, ed. *Fretting Fatigue*. London: Elsevier Applied Science; 1981:99.
6. Waterhouse RB. Fretting Corrosion. *Proc Inst Mech Eng*. 1955;169(1):1157-1172. doi:10.1243/PIME_PROC_1955_169_112_02
7. Bill RC. The Role of Oxidation in the Fretting Wear Process. *NASA Met Mater*. 1980. doi:NASA-TM-81570, AVRADCOM-TR-80-C-15, E-538
8. Brown SA, Flemming CAC, Kawalec JS, et al. Fretting corrosion accelerates crevice corrosion of modular hip tapers. *J Appl Biomater*. 1995;6(1):19-26. doi:10.1002/jab.770060104
9. Goldberg JR, Gilbert JL, Jacobs JJ, Bauer TW, Paprosky W, Leurgans S. A Multicenter Retrieval Study of the Taper Interfaces of Modular Hip Prostheses. *Clin Orthop Relat Res*. 2002;401:149-161. doi:10.1097/00003086-200208000-00018
10. Vingsbo O, Söderberg S. On fretting maps. *Wear*. 1988;126(2):131-147. doi:10.1016/0043-1648(88)90134-2

11. Zhou ZR, Nakazawa K, Zhu MH, Maruyama N, Kapsa P, Vincent L. Progress in fretting maps. *Tribol Int*. 2006;39(10):1068-1073. doi:10.1016/j.triboint.2006.02.001

12. Mindlin RD, Deresiewicz H. Elastic spheres in contact under varying oblique forces. *ASME Tram J Appl Mech*. 1953;20:327-344.

13. Zhou ZR, Vincent L. Mixed fretting regime. *Wear*. 1995;181-183(PART 2):531-536. doi:10.1016/0043-1648(95)90168-X

14. Fouvry S, Kapsa P, Vincent L. Developments of fretting sliding criteria to quantify the local friction coefficient evolution under partial slip condition. In: Elsevier; 1998:161-172. doi:10.1016/S0167-8922(98)80071-0

15. Fouvry S, Kapsa P, Zahouani H, Vincent L. Wear analysis in fretting of hard coatings through a dissipated energy concept. *Wear*. 1997;203-204(96):393-403. doi:10.1016/S0043-1648(96)07436-4

16. Fouvry S, Kapsa P, Vincent L. Description of fretting damage by contact mechanics. *ZAMM - J Appl Math Mech / Zeitschrift für Angew Math und Mech*. 2000;80(S1):41-44. doi:10.1002/zamm.20000801311

17. Fouvry S, Kapsa P, Vincent L. Analysis of sliding behaviour for fretting loadings: determination of transition criteria. *Wear*. 1995;185(1-2):35-46. doi:10.1016/0043-1648(94)06582-9

18. Bryant M, Neville A. Fretting corrosion of CoCr alloy: Effect of load and displacement on the degradation mechanisms. *Proc Inst Mech Eng Part H J Eng Med*. 2017;231(2):114-126. doi:10.1177/0954411916680237

19. Heredia S, Fouvry S. Introduction of a new sliding regime criterion to quantify partial, mixed and gross slip fretting regimes: Correlation with wear and cracking processes. *Wear*. 2010;269(7-8):515-524. doi:10.1016/j.wear.2010.05.002

20. Suciu CV, Uchida T. Modeling and Simulation of the Fretting Hysteresis Loop. In: *2010 International Conference on P2P, Parallel, Grid, Cloud and Internet Computing*. IEEE; 2010:560-564. doi:10.1109/3PGCIC.2010.96

21. Varenberg M, Etsion I, Halperin G. Slip Index: A New Unified Approach to Fretting. *Tribol Lett*. 2004;17(3):569-573. doi:10.1023/B:TRIL.0000044506.98760.f9

22. Hartman WF. Towards Standards for Acoustic Emission Technology. In: Symposium on Nondestructive Testing Standards; Berger HUSAS for T, ed. *Nondestructive Testing Standards : A Review : A Symposium*. ASTM; 1977:138-145.

23. Matsuoka K, Taniguchi K, Nakakita M. In-Situ Wear Monitoring of Slider and Disk Using Acoustic Emission. *J Tribol*. 2001;123(1):175-180. doi:10.1115/1.1327586

24. Ravindra HV, Srinivasa YG, Krishnamurthy R. Acoustic emission for tool condition monitoring in metal cutting. *Wear*. 1997;212(1):78-84. doi:10.1016/S0043-1648(97)00137-3

25. Tandon N, Choudhury A. A review of vibration and acoustic measurement methods for the detection of defects in rolling element bearings. *Tribol Int*. 1999;32(8):469-480. doi:10.1016/S0301-679X(99)00077-8

26. BSI. BS EN 1330-9 Non-destructive testing - Terminology - Part 9: Terms used in acoustic emission testing. *BSI*. 2017.

27. Meriaux J, Boinet M, Fouvry S, Lenain JC. Identification of fretting fatigue crack propagation mechanisms using acoustic emission. *Tribol Int*. 2010;43(11):2166-2174.

doi:10.1016/j.triboint.2010.06.009

28. Higgens FP, Carpenter SH. Sources of acoustic emission generated during the tensile deformation of pure iron. *Acta Metall*. 1978;26(1):133-139. doi:10.1016/0001-6160(78)90209-2

29. Ukpai JI, Barker R, Hu X, Neville A. Determination of particle impacts and impact energy in the erosion of X65 carbon steel using acoustic emission technique. *Tribol Int*. 2013;65:161-170. doi:10.1016/j.triboint.2013.03.012

30. Ferrer C, Salas F, Pascual M, Orozco J. Discrete acoustic emission waves during stick–slip friction between steel samples. *Tribol Int*. 2010;43(1-2):1-6. doi:10.1016/j.triboint.2009.02.009

31. Han Z, Luo H, Cao J, Wang H. Acoustic emission during fatigue crack propagation in a micro-alloyed steel and welds. *Mater Sci Eng A*. 2011;528(25-26):7751-7756. doi:10.1016/j.msea.2011.06.065

32. Hase A, Wada M, Mishina H. Acoustic Emission Signals and Wear Phenomena on Severe-Mild Wear Transition. *Tribol Online*. 2008;3(5):298-303. doi:10.2474/trol.3.298

33. Hase A, Mishina H, Wada M. Correlation between features of acoustic emission signals and mechanical wear mechanisms. *Wear*. 2012;292-293:144-150. doi:10.1016/j.wear.2012.05.019

34. Asamene K, Sundaresan M. Analysis of experimentally generated friction related acoustic emission signals. *Wear*. 2012;296(1-2):607-618. doi:10.1016/j.wear.2012.07.019

35. Couturier J, Mba D. Operational Bearing Parameters and Acoustic Emission Generation. *J Vib Acoust*. 2008;130(2):1-5. doi:10.1115/1.2776339

36. Wang D, Zhang D, Ge S. Effect of displacement amplitude on fretting fatigue behavior of hoisting rope wires in low cycle fatigue. *Tribol Int*. 2012;52:178-189. doi:10.1016/j.triboint.2012.04.008

37. Cadario A, Alfredsson B. Fretting fatigue experiments and analyses with a spherical contact in combination with constant bulk stress. *Tribol Int*. 2006;39(10):1248-1254. doi:10.1016/j.triboint.2006.02.012

38. Ito S, Shima M, Jibiki T, Akita H. The relationship between AE and dissipation energy for fretting wear. *Tribol Int*. 2009;42(2):236-242. doi:10.1016/j.triboint.2008.06.010

39. Benítez A, Denape J, Paris J-Y. Interaction between systems and materials in fretting. *Wear*. 2016;368-369:183-195. doi:10.1016/j.wear.2016.09.012

40. Merhej R, Beguin JD, Paris J-Y, Denape J. Acoustic emission for investigations on fretting wear of ceramic-metal contacts. *Eur Conf Tribol*. 2009;1(June):1-6.

41. Briscoe BJ, Chateauminois A, Chiu J, Vickery S. Acoustic noise emission in a model PMMA/steel fretting contact. In: *Tribology Research*. Vol 39. ; 2001:673-681. doi:10.1016/S0167-8922(01)80149-8

42. Ben Abdelounis H, Zahouani H, Le Bot A, Perret-Liaudet J, Tkaya M Ben. Numerical simulation of friction noise. *Wear*. 2011;271(3-4):621-624. doi:10.1016/j.wear.2010.07.014

43. Sauger E, Fouvry S, Ponsonnet L, Kapsa P, Martin J., Vincent L. Tribologically transformed structure in fretting. *Wear*. 2000;245(1-2):39-52. doi:10.1016/S0043-1648(00)00464-6

44. Wade A, Copley R, Alsheikh Omar A, Clarke B, Liskiewicz T, Bryant M. Novel numerical method for parameterising fretting contacts. *Tribol Int*. June 2019:105826.

doi:10.1016/j.triboint.2019.06.019

45. Geng Z, Puhan D, Reddyhoff T. Using acoustic emission to characterize friction and wear in dry sliding steel contacts. *Tribol Int*. 2019;134(February):394-407. doi:10.1016/j.triboint.2019.02.014